



## Direct observations of blob deformation during a substorm

T. Ishida<sup>1,2</sup>, Y. Ogawa<sup>1,2</sup>, A. Kadokura<sup>1,2</sup>, K. Hosokawa<sup>3</sup>, and Y. Otsuka<sup>4</sup>

<sup>1</sup>National Institute of Polar Research, Tokyo 190-8518, Japan

<sup>2</sup>Department of Polar Science, SOKENDAI (The Graduate University for Advanced Studies), Tokyo 190-8518, Japan

<sup>3</sup>Department of Communication Engineering and Informatics, University of Electro-Communications, Tokyo 182-8585, Japan

<sup>4</sup>Solar-Terrestrial Environment Laboratory, Nagoya University, Nagoya 464-8601, Japan

Correspondence to: T. Ishida (ishida.tetsuro@nipr.ac.jp)

Received: 14 October 2014 – Revised: 25 February 2015 – Accepted: 17 April 2015 – Published: 6 May 2015

**Abstract.** Ionospheric blobs are localized plasma density enhancements, which are mainly produced by the transportation process of plasma. To understand the deformation process of a blob, observations of plasma parameters with good spatial–temporal resolution are desirable. Thus, we conducted the European Incoherent Scatter radar observations with high-speed meridional scans (60–80 s) during October and December 2013, and observed the temporal evolution of a blob during a substorm on 4 December 2013. This paper is the first report of direct observations of blob deformation during a substorm. The blob deformation arose from an enhanced plasma flow shear during the substorm expansion phase, and then the blob split into two smaller-scale blobs, whose scale sizes were more than  $\sim 100$  km in latitude. Our analysis indicates that the Kelvin–Helmholtz instability and dissociative recombination could have deformed the blob structure.

**Keywords.** Ionosphere (ionospheric irregularities)

### 1 Introduction

Localized plasma density enhancements are often produced in the high-latitude ionosphere by the transportation process of plasma or particle precipitations. Among such plasma density enhancements, structures enhanced by a factor of 2–10 above the background density, and with horizontal dimensions ranging from  $\sim 100$  to 1000 km, are generally called patches in the polar cap, or blobs outside of the polar cap (e.g., Tsunoda, 1988; Crowley et al., 2000). The blobs

are generally categorized into the following three types: (1) boundary blobs, (2) subauroral blobs, and (3) auroral blobs. Boundary blobs are regarded as a proxy of the equatorward auroral boundary. Subauroral blobs resemble boundary blobs but are found in the trough region. In contrast, auroral blobs are observed in the auroral oval, and they appear to be localized in longitude when compared with boundary and subauroral blobs. Blobs/patches are important research subjects because they turn into ionospheric irregularities through some sort of deformation processes, and these irregularities affect radio wave propagation and scintillation of Global Navigation Satellite System (GNSS) signals (e.g., Moen et al., 2013; Jin et al., 2014). Blobs/patches are known to be created by temporal/spatial changes in the convection pattern (e.g., Livingstone et al., 1982; Crowley et al., 2000; Hosokawa et al., 2010a). Besides, high-speed plasma flow can also deform them through the enhanced dissociative recombination process (Valladares et al., 1994). Thus, it is clear that background plasma convection plays an important role in blob deformation. However, detailed blob behavior (deformation/splitting) under highly variable plasma convection during substorms is still unclear because of the lack of adequate observations. Therefore, new techniques that can follow variations of plasma parameters (e.g., density, velocity, and temperature) in detail are highly desirable.

In past studies, large-scale ionospheric density structures including blobs have been investigated using ground-based global positioning system (GPS) receivers to obtain TEC (total electron content) maps (e.g., Coster et al., 2003; Foster et al., 2005; Hosokawa et al., 2010b; Zhang et al., 2013). The TEC maps can provide visualizations of the temporal evo-

lution of the large-scale ionospheric density structure, but they cannot resolve the small-scale structure because of their limited spatial–temporal resolution (grid resolution of  $1^\circ$  for the latitude and  $2^\circ$  for the longitude, temporal resolution of 5 min). Furthermore, to study the blob deformation process in detail, we need to know not only the plasma structure but also the motion of the plasma convection with sufficient temporal resolution. Therefore, we conducted the European Incoherent Scatter (EISCAT) radar observations with high-speed meridional scans (grid resolution of  $\sim 0.1\text{--}0.5^\circ$  for the latitude, temporal resolution of 60–80 s) during October and December 2013. In this campaign, we encountered a convected blob inside the high-latitude trough in the pre-midnight to dusk region. The blob was deformed during a substorm. In this study, we examine the temporal evolution of the blob structure using the EISCAT data and other complementary data such as TEC maps and ground-based magnetometer data.

## 2 Observations

The high-speed meridional scans of the EISCAT UHF radar take 60–80 s to scan elevation angles from  $25$  to  $89^\circ$ . The EISCAT UHF radar is located in Tromsø, northern Norway ( $69^\circ 35' \text{ N}$ ,  $19^\circ 14' \text{ E}$ ; invariant latitude:  $66^\circ 12' \text{ N}$ ), and this observatory collects information on the following ionospheric plasma parameters: electron density ( $N_e$ ), ion temperature ( $T_i$ ), electron temperature ( $T_e$ ), and line-of-sight ion velocity ( $V_{i(\text{LOS})}$ ). The observations were conducted as part of the peer-reviewed program (PP) and Japanese Special Program (SP) during October and December 2013, and we obtained a total of nine events that each lasted for a period of 4 h (14:00–18:00 UT, MLT  $\simeq$  UT + 2.2 h). To date, the EISCAT observations of the blob have been conducted mainly by Common Program 3 (CP-3) scans, which take  $\sim 30$  min for a single scan. However, as the temporal resolution of these single scans was insufficient to observe the rapid variation of the blob, we developed high-speed meridional scans for this study, with a temporal resolution that is  $\sim 25$  times higher than that of the CP-3 scans. A detailed description of the CP-3 scans was introduced in an earlier publication (see Ishida et al., 2014, Fig. 1). Since the EISCAT observations cannot capture the large-scale picture around the field of view (FOV) due to its limited observational range (up to  $\sim 5^\circ$  of the latitude), we used TEC maps to visualize the horizontal shape of the density structures. In addition, the convection pattern around the EISCAT FOV was inferred from the ground-based magnetometer data.

During the observation campaign, we encountered a substorm on 4 December 2013 at 17:00–18:00 UT, which was detected using the geomagnetic data. The beginning of the negative bay was shown at  $\sim 17:00$  UT in the magnetometer H-component of Dixon Island ( $73.54^\circ \text{ N}$ ,  $80.56^\circ \text{ E}$ ) and Tixie Bay ( $71.58^\circ \text{ N}$ ,  $129.00^\circ \text{ E}$ ) located in the magnetic mid-

night sector, which means that the substorm growth phase started at this time. Subsequently, it explosively developed at  $\sim 17:30$  UT; at the same time, Pi2 pulsation also appeared at Nurmijärvi ( $56.89^\circ \text{ N}$ ,  $102.18^\circ \text{ E}$ ). Moreover, the auroral electrojet (AE) index suddenly increased at  $\sim 17:35$  UT. Thus, we concluded that the onset time was around 17:30 UT. The interplanetary magnetic field (IMF) was predominantly southward ( $-4.4$  to  $-3.4$  nT) during 17:00–18:00 UT. In addition, the IMF  $B_y$  component turned from positive to negative (down to  $\sim -2.0$  nT) at  $\sim 17:40$  UT.

## 3 Results

Figure 1 shows the TEC maps after onset of the substorm. The color scale runs from a high-electron density (red) to a low-electron density (blue). The top left panel of Fig. 1 is an overview of the polar ionosphere around onset time ( $\sim 17:30$  UT). The dashed black line represents the solar terminator, where  $\text{SZA} = 90^\circ$ . Besides, the top right panel is the TEC variation around the EISCAT FOV, which enlarges the black box shown in the top left panel. The black rectangle indicates the EISCAT FOV, and the dashed curving line indicates the boundary of the high-latitude trough. The earlier study used a threshold of just 20 % lower than the background ionospheric electron density to identify the ionospheric trough (Ishida et al., 2014). In this event, therefore, the region of less than  $\sim 4.8$  TECU (total electron content unit;  $1 \text{ TECU} = 10^{16} \text{ el m}^{-2}$ ) can be considered as the trough region since the background ionospheric electron density was  $\sim 6.0$  TECU in the nightside. Thus, we can see that the EISCAT FOV was inside of the trough region after onset of the substorm. Figure 1a–f show a time sequence of the horizontal shape of the density structures around the EISCAT FOV. Note that the color scale ranges within 0.5–3.5 TECU so that the focus is on the density variation in the trough region. A sequence of structural change shown in Fig. 1a–c illustrates that a chunk of increased plasma density gets closer to the EISCAT radar during 17:30–17:45 UT, and thus the TEC value slightly increases around the high-latitude side of the EISCAT FOV (up to  $\sim 3$  TECU in Fig. 1c). Then, the horizontal shape changes intricately around the EISCAT FOV during 17:45–18:00 UT (d–f). As described above, the TEC maps indicate that the EISCAT radar observed the plasma structuring in the pre-midnight to dusk subauroral region, and the structuring was shown in the trough region. Thus, the blob deformation, which is shown in detail later, likely can be regarded as that of a subauroral blob.

Figure 2 shows the keogram at an altitude of 210 km that was reproduced from the  $N_e$  observed by the meridional scans, with overplotted convection vectors. A keogram is the time versus geomagnetic latitude plot of the EISCAT plasma parameters along a specific cross section. In this study, we show a keogram along the geomagnetic north–south cross section. The convection vectors were from the Inter-

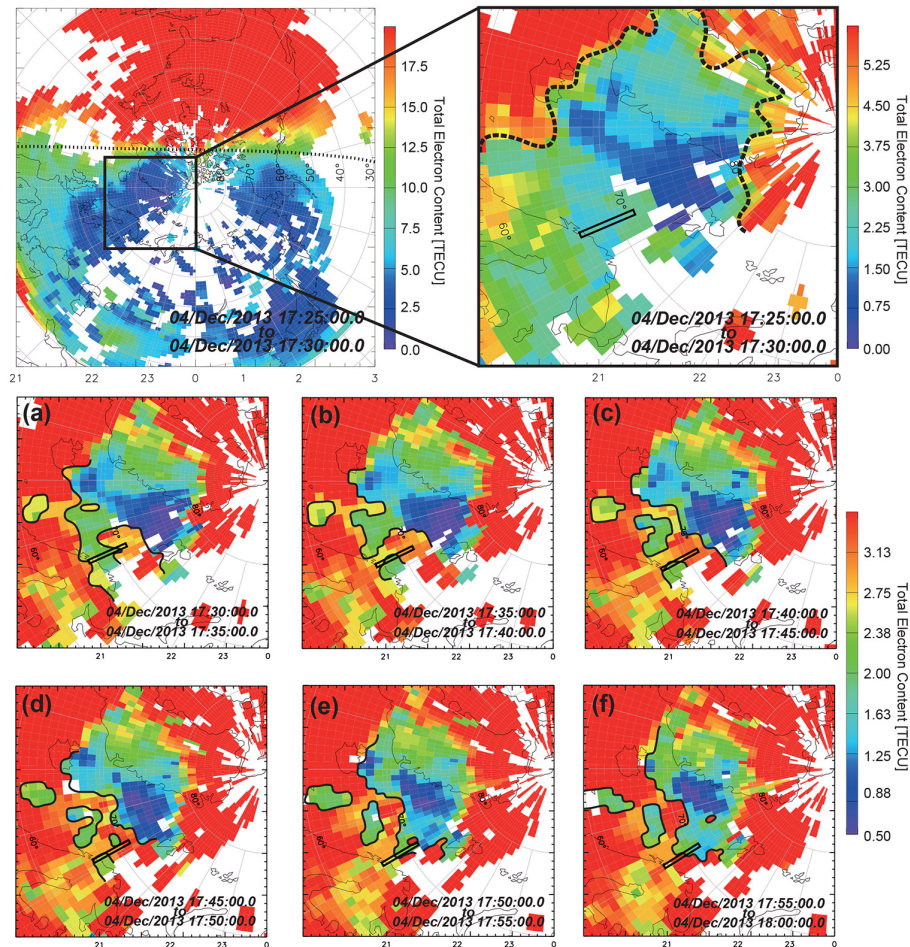
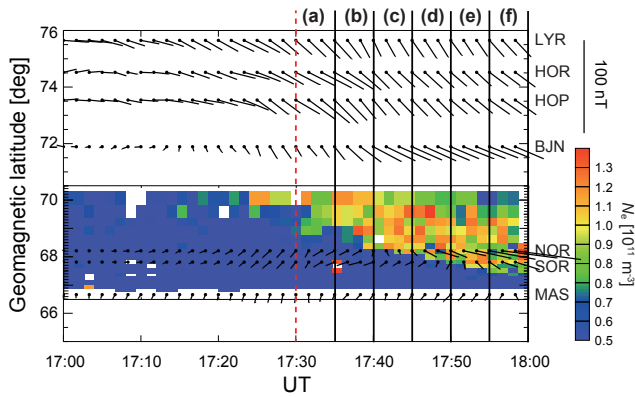


**Figure 1.** The TEC map after onset of the substorm. The top left panel is an overview of the polar ionosphere around onset time, and the top right panel enlarges the black box shown in the top left panel; these data represent the TEC variation around the EISCAT FOV. The color scale runs from high-electron density (red) to low-electron density (blue). The dashed black line in the top left panel represents the solar terminator, where  $SZA = 90^\circ$ . The black rectangle in the top right panel indicates the EISCAT FOV, and the dashed curving line indicates the boundary of the high-latitude trough. (a–f) indicate a time sequence of the horizontal shape of the density structures around the EISCAT FOV. The median filter was applied to each TEC map.

national Monitor for Auroral Geomagnetic Effects (IMAGE) meridian chain (see station information at <http://space.fmi.fi/image/beta/?page=maps>). Note that the convection vectors are in the opposite direction from the equivalent current vectors derived from the IMAGE magnetometer data and the vector size does not reflect the actual drift speed but the geomagnetic variation. The red dashed vertical line indicates the onset time of the substorm ( $\sim 17:30$  UT), and the remaining 30 min is divided into six sections according to Fig. 1a–f. A high-density blob appears at  $\sim 17:20$  UT, and then it extends toward the low-latitude region by the end of the observations (18:00 UT). The overplotted vectors shown in Fig. 2 indicate that the southeastward flow was dominant above  $\sim 71.5^\circ$  N, while the southwestward flow was dominant below  $\sim 68.5^\circ$  N during 17:00–17:40 UT. Therefore, we can say that a southeast–southwest flow shear existed between  $68.5^\circ$  N and  $71.5^\circ$  N at least by  $\sim 17:40$  UT.

Since the southeastward flow region expanded equatorward from  $\sim 17:20$  UT to 18:00 UT, the latitude of the flow shear seemed to move over time, and it appeared to be located at a lower latitude than the blob region after  $\sim 17:50$  UT. In addition, it should be noted that the southeastward flow increased rapidly at  $\sim 68^\circ$  N after  $\sim 17:50$  UT.

Figure 3 shows the temporal evolution of a blob on the meridional plane during Fig. 1e–f: (top)  $N_e$ , (middle) north–south component of ion velocity ( $V_{i(N-S)}$ ), and (bottom)  $T_i$ . Note that the  $V_{i(N-S)}$  was calculated from the  $V_{i(LOS)}$  and the elevation angle of the meridional scan. Dashed slant lines indicate the geomagnetic field lines. Red horizontal axes indicate the geomagnetic latitudes at an altitude of 210 km. Hereafter, unless otherwise noted, the geomagnetic latitude refers to that in Fig. 3. Since the  $V_{i(LOS)}$  and  $T_i$  deduced from incoherent scatter fitting are usually inappropriate in the case of  $N_e < 5 \times 10^{10} \text{ m}^{-3}$ , we ignored them in such situations.



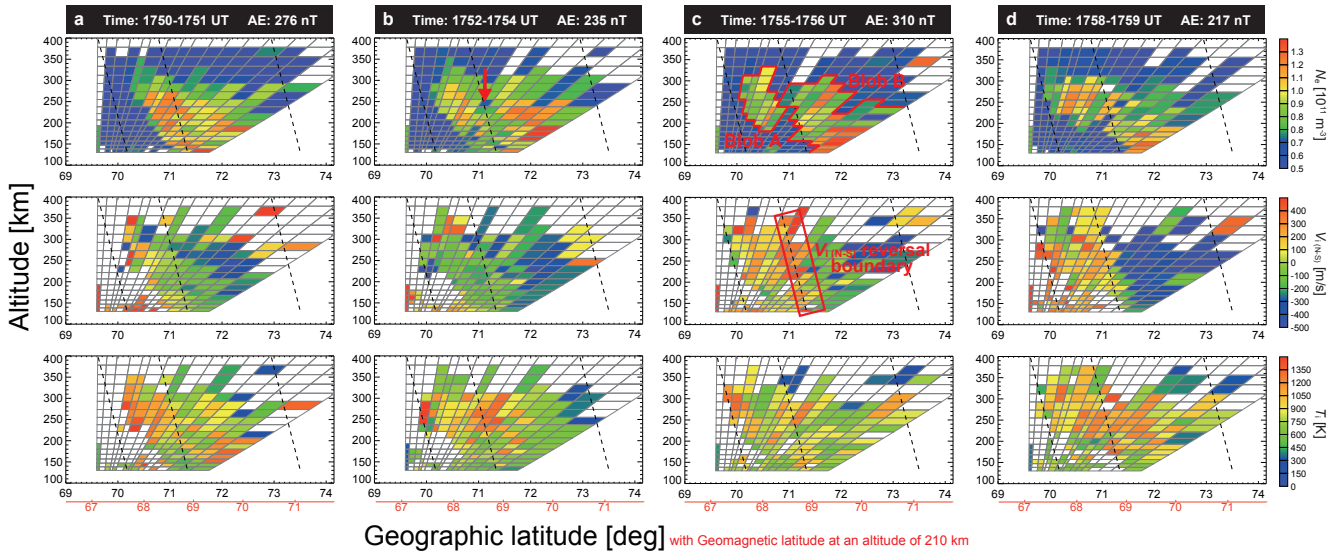
**Figure 2.** Observations from EISCAT and the IMAGE magnetometer during the substorm on 4 December 2013. The keogram was reproduced from the  $N_e$  observed by the meridional scans at an altitude of 210 km, with overplotted convection vectors at an altitude of 120 km from the IMAGE meridian chain. The red dashed vertical line indicates the onset time ( $\sim 17:30$  UT), and the remaining 30 min is divided into six sections according to Fig. 1a–f.

Figure 3a shows that a part of the blob appears at the high-latitude side of the EISCAT FOV, which was nearly superposed on the region of southward velocity. Figure 3b–c show that the blob seems to be cracked around  $68.5^\circ$  N (red arrow in Fig. 3b) at  $\sim 17:52$  UT, and then it is clearly divided into two parts (Blob A and Blob B) over the boundary where the  $V_{i(N-S)}$  reversed from northward to southward (hereafter referred to as the  $V_{i(N-S)}$  reversal boundary), whose northward component reaches to  $\sim 400$ – $500$   $\text{m s}^{-1}$ . The scale sizes of the divided blobs were  $\sim 100$  km in latitude (Blob A) and more than 250 km in latitude (Blob B). It can also be seen that the  $V_{i(N-S)}$  reversal boundary was roughly along the geomagnetic field line. Blob A was distributed at altitudes between 180 and 300 km, while blob B was distributed at even lower altitudes. Furthermore, the cross section between the two blobs was roughly along the geomagnetic field line. Figure 3d shows that the divided blobs appear to be elongated equatorward, and the velocity difference on the  $V_{i(N-S)}$  reversal boundary reached to  $\sim 800$   $\text{m s}^{-1}$ . Another feature identified in Fig. 3 is that the  $T_i$  partially increased around the location where the blob started to be divided in Fig. 3b, and the values reached up to  $\sim 1400$  K.

#### 4 Discussion

In this section, we evaluate the physical and chemical processes associated with the blob deformation shown in Fig. 3. Figure 4 shows the horizontal distribution of the convection vectors at  $\sim 17:55$  UT (the time when the blob deformation was observed). The green, red, and black vectors are the convection vectors from the IMAGE magnetometer. The southeastward flow (green vectors) was located at the east side of the EISCAT radar, while the southwestward

flow (red vectors) was located at the low-latitude side. From the above circumstances, we presumed that southeastward–northwestward flow shear was located around the EISCAT observational region. As mentioned in Sect. 3, the  $V_{i(N-S)}$  was southward at the high-latitude side of the FOV, while it was northward at the low-latitude side of the FOV at  $\sim 17:55$  UT. Thus, we assumed here that EISCAT observed the localized northwestward flow (a large red arrow in Fig. 4) accompanied by southeastward–northwestward flow shear. It is known that the plasma flow shear is enhanced in the pre-midnight to dusk region during the substorm expansion phase (e.g., Iijima and Nagata, 1972). Such plasma flow shear is considered to be formed by a combination of the DP 2 field (convection current system) and DP 1 field (substorm current system) (see Iijima and Nagata, 1972, Fig. 9). Moreover, a statistical analysis using SuperDARN data also indicated that the zonal convection speed is enhanced in the pre-midnight to dusk region during the substorm expansion phase in the case of  $\text{IMF } B_y < 0$  (see Grocott et al., 2010, Fig. 4d). Hence, if EISCAT actually observed the enhanced plasma flow shear accompanied by the substorm expansion phase, the blob deformation might have been caused by the enhanced flow shear through the Kelvin–Helmholtz instability (KHI). Thus, we investigated the possibility that the blob deformation was caused by the enhanced flow shear through the KHI. To evaluate the blob deformation in a quantitative way, we calculated the linear growth rate of the KHI on the basis of some assumptions. Early studies used  $0.2 V/L$  as the linear growth rate of the KHI, and thus the growth time  $\tau_{KH}$  turns out to be  $5 L/V$ , which is the inverse of the growth rate (Carlson et al., 2007). Here,  $V$  is the velocity difference and  $L$  is the scale length of the velocity difference. As shown in the line plot of Fig. 4, the  $V_{i(N-S)}$  reverses sharply from  $\sim 450$   $\text{m s}^{-1}$  (northward) to  $\sim -300$   $\text{m s}^{-1}$  (southward) between  $68$  and  $69^\circ$  N along the geomagnetic field line. Assuming that the velocity difference on the  $V_{i(N-S)}$  reversal boundary is derived from the zonal (southeastward–northwestward) flow shear, we can find that the scale length  $L$  is  $\sim 0.8^\circ$  of the latitude (see dashed red rectangle in Fig. 4), which corresponds to  $\sim 90$  km at an altitude of 210 km. Considering that the blob starts to deform at  $\sim 17:52$  UT, the KHI would have grown during  $\sim 3$ – $4$  min ( $\sim 3.5$  min on average) by the time of Fig. 3c. Thus, we can find that the velocity difference of the convection shear  $V_{i(\text{shear})}$  has to be larger than  $\sim 2100$   $\text{m s}^{-1}$  by the equation  $\tau_{KH} \leq 3.5 \text{ min} \Rightarrow V \geq 5 \times 90 \text{ km}/3.5 \text{ min}$ . Plasma flows of thousands of meters per second are often observed during substorms (e.g., Zesta et al., 2011). If such zonal (southeastward–northwestward) flow shear really existed, the angle  $\theta$  between the shear plane and meridional plane must be larger than  $\sim 70^\circ$  according to the equation  $V_{i(\text{shear})} = V_{i(N-S)}/\cos(\theta) \geq 2100$  [ $\text{m s}^{-1}$ ], with  $V_{i(N-S)} \sim 750$  [ $\text{m s}^{-1}$ ] around the shear region. Besides, Fig. 4 indicates that the angle  $\theta$  is seemingly larger than  $\sim 70^\circ$  around the EISCAT FOV; in addition, Figure 2 also shows the convection vectors are inclined larger than  $\sim 70^\circ$



**Figure 3.** The temporal evolution of a blob on the meridional plane during Fig. 1e–f, with geographic latitudes on the horizontal axes and altitudes on the vertical axes: (top)  $N_e$ , (middle)  $V_{i(N-S)}$ , and (bottom)  $T_i$ . Dashed slant lines indicate the geomagnetic field lines. Red horizontal axes indicate the geomagnetic latitudes at an altitude of 210 km.

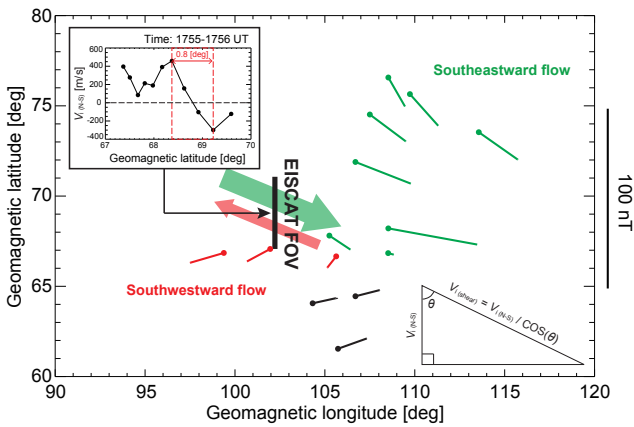


**Figure 4.** The horizontal distribution of the convection vectors at  $\sim 17:55$  UT. The green, red, and black vectors are the convection vectors from the IMAGE magnetometer. The large red arrow indicates the localized northwestward flow, which was assumed from the horizontal distribution of the convection vector and EISCAT data. The line plot shows the latitudinal variation of the  $V_{i(N-S)}$  at  $\sim 17:55$  UT.

from the meridional plane after  $\sim 17:52$  UT around  $68^\circ$  N, which also support the above assumption. Hence, it is possible that the KHI could play a role in modulating the blob structure under the above assumption, although this is not a conclusive answer for the blob deformation.

Next, we discuss the extent to which chemical processes could have influenced the blob deformation. As mentioned in Sect. 3, it was found that the  $T_i$  partially increased around the location where the blob started to be divided in Fig. 3b.

In such a case, there is the possibility that frictional heating will cause blob cutting if the dissociative recombination promotion is fast enough at the localized heated region. An early study indicated that the tongue of ionization (TOI) was divided into two patches by high-speed plasma jets in excess of  $2 \text{ km s}^{-1}$  through the enhanced recombination process (Valladares et al., 1994). Since we could identify that the blob deformed at  $\sim 150\text{--}300$  km altitudes from Fig. 3b–c, we compared the recombination rates by altitude to evaluate whether or not dissociative recombination could have promoted this on a timescale of minutes. The recombination rate  $\beta$  used here was estimated from the mass spectrometer incoherent scatter (MSIS) model parameters and theoretical equations introduced by St.-Maurice and Torr (1978). Note that for simplicity, we used a recombination rate for/at  $T_i = \sim 1400$  K at all altitudes. Then, we can confirm that  $\beta$  is nearly equal to  $\sim 310 \times 10^{-4} \text{ s}^{-1}$  at 150 km,  $\sim 58 \times 10^{-4} \text{ s}^{-1}$  at 180 km,  $\sim 16 \times 10^{-4} \text{ s}^{-1}$  at 210 km, and  $\sim 5 \times 10^{-4} \text{ s}^{-1}$  at 240 km, which correspond to recombination times of  $\sim 0.5$  min,  $\sim 3$  min,  $\sim 10$  min, and  $\sim 33$  min, respectively. Considering that the blob starts to deform at  $\sim 17:52$  UT, the dissociative recombination process would have been promoted for  $\sim 3\text{--}4$  min by the time of Fig. 3c. Hence, the results indicate that there would have been sufficient recombination time to allow for dissociative recombination and the blob cutting scenario at roughly less than 180 km of altitude, but it is difficult to explain that at higher altitudes.

## 5 Conclusions

To the best of our knowledge, this is the first detailed report containing direct observations of blob deformation at the nightside auroral region during a substorm, and our report is accompanied by an evaluation of the plausible processes that could have contributed to blob deformation. During the substorm expansion phase, the blob seems to have divided into two parts, whose scale sizes were more than  $\sim 100$  km of the latitude. We then discussed the possible physical and chemical processes that may have caused this blob deformation. Our analysis indicated that the KHI and dissociative recombination could have influenced the blob structure.

**The Supplement related to this article is available online at doi:10.5194/angeocom-33-525-2015-supplement.**

*Acknowledgements.* This research was financially supported by the Japan Society for the Promotion of Science (JSPS) Fellows program and the Center for the Promotion of Integrated Sciences (CPIS) of SOKENDAI. We are indebted to the director and staff of EISCAT for providing the observational data. EISCAT is an international association supported by research organizations in China (CRIRP), France (CNRS, until the end of 2006), Finland (SA), Germany (DFG, until the end of 2011), Japan (NIPR and STEL), Norway (NFR), Sweden (VR), and the United Kingdom (NERC). Ingemar Häggström is also acknowledged for his helpful support in operating the EISCAT peer-reviewed program experiments and special experiments in Tromsø.

The authors are thankful for the GPS-TEC data that were collected under the direction of A. J. Coster at the MIT Haystack Observatory. The TEC map was obtained from the GPS/TEC Plot routine on the Virginia Tech SuperDARN website (<http://vt.superdarn.org/tiki-index.php?page=DaViT+TEC>), which is supported by NSF award numbers AGS-0838219 and AGS-0946900.

The IMAGE magnetometer network is maintained by 10 institutes from Estonia, Finland, Germany, Norway, Poland, Russia, and Sweden. The authors are grateful for their continuous effort in maintaining the receivers.

The topical editor Steve Milan thanks one anonymous referee for help in evaluating this paper.

## References

- Carlson, H. C., Pedersen, T., Basu, S., Keskinen, M., and Moen, J.: Case for a new process, not mechanism, for cusp irregularity production, *J. Geophys. Res.*, 112, A11304, doi:10.1029/2007JA012384, 2007.
- Coster, A., Foster, F. C., and Erickson, P.: Monitoring the ionosphere with GPS: Space weather, *GPS World*, 14, 42–49, 2003.
- Crowley, G., Ridley, A. J., Deist, D., Wing, S., Knipp, D. J., Emery, B. A., Foster, J., Heelis, R., Hairston, M., and Reinisch, B. W.: The transformation of high-latitude ionospheric F-region patches into blobs during the 21 March 1990 storm, *J. Geophys. Res.*, 105, 5215, 2000.
- Foster, J. C., Coster, A. J., Erickson, P. J., Holt, J. M., Lind, F. D., Rideout, W., McCready, M., van Eyken, A., Greenwald, R. A., and Rich, F. J.: Multiradar observations of the polar tongue of ionization, *J. Geophys. Res.*, 110, A09S31, doi:10.1029/2004JA010928, 2005.
- Grocott, A., Milan, S. E., Yeoman, T. K., Sato, N., Yukimatu, A. S., and Wild, J. A.: Superposed epoch analysis of the ionospheric convection evolution during substorms: IMF  $B_y$  dependence, *J. Geophys. Res.*, 115, A00I06, doi:10.1029/2010JA015728, 2010.
- Hosokawa, K., St.-Maurice, J. P., Sofko, G. J., Shiokawa, K., Otsuka, Y., and Ogawa, T.: Reorganization of polar cap patches through shears in the background plasma convection, *J. Geophys. Res.*, 115, A01303, doi:10.1029/2009JA014599, 2010a.
- Hosokawa, K., Tsugawa, T., Shiokawa, K., Otsuka, Y., Nishitani, N., Ogawa, T., and Hairston, M. R.: Dynamic temporal evolution of polar cap tongue of ionization during magnetic storm, *J. Geophys. Res.*, 115, A12333, doi:10.1029/2010JA015848, 2010b.
- Iijima, T. and Nagata, T.: Signatures for the substorm development of the growth phase and expansion phase, *Planet. Space Sci.*, 20, 1095–1101, 1972.
- Ishida, T., Ogawa, Y., Kadokura, A., Hiraki, Y., and Häggström, I.: Seasonal variation and solar activity dependence of the quiet-time ionospheric trough, *J. Geophys. Res.*, 119, doi:10.1002/2014JA019996, 2014.
- Jin Y., Moen, J. I., and Miloch, W. J.: GPS scintillation effects associated with polar cap patches and substorm auroral activity: direct comparison, *J. Space Weather Space Clim.*, 4, doi:10.1051/swsc/2014019, 2014.
- Livingston, R. C., Rino, C. L., Owen, J., and Tsunoda, R. T.: The anisotropy of high-latitude nighttime F region irregularities, *J. Geophys. Res.*, 87, 10519–10526, doi:10.1029/JA087iA12p10519, 1982.
- Moen, J., Oksavik, K., Alfonsi, L., Daabakk, Y., Romano, V., and Spogli, L.: Space weather challenges of the polar cap ionosphere, *J. Space Weather Space Clim.*, 3, doi:10.1051/swsc/2013025, 2013.
- St.-Maurice, J.-P. and Torr, D.: Nonthermal rate coefficients in the ionosphere: The reactions of  $O^+$  with  $N_2$ ,  $O_2$ , and  $NO$ , *J. Geophys. Res.*, 83, 969–977, 1978.
- Tsunoda, R. T.: High-latitude F region irregularities: A review and synthesis, *Rev. Geophys.*, 26, 719–760, 1988.
- Valladares, C. E., Basu, S., Buchau, J., and Friis-Christensen, E.: Experimental evidence for the formation and entry of patches into the polar cap, *Radio Sci.*, 29, 167–194, 1994.
- Zesta, E., et al.: Ionospheric convection signatures of tail fast flows during substorms and Poleward Boundary Intensifications (PBI), *Geophys. Res. Lett.*, 38, L08105, doi:10.1029/2011GL046758, 2011.
- Zhang, Q., Zhang, B., Lockwood, M., Hu, H., Moen, J., Ruohoniemi, J. M., Thomas, E. G., Zhang, S., Yang, H., Liu, R., McWilliams, K. A., and Baker, J. B. H.: Direct observations of the evolution of polar cap ionization patches, *Science*, 339, 1597–1600, doi:10.1126/science.1231487, 2013.